Ultramicroscopy 000 (2017) 1–7

Contents lists available at ScienceDirect

Ultramicroscopy

journal homepage: www.elsevier.com/locate/ultramic

Rapid measurement of low-order aberrations using Fourier transforms of crystalline Ronchigrams

Koji Kimoto[a,*], Kazuo Ishizuka[b]

[a] National Institute for Materials Science, 1-1 Namiki, Tsukuba, Ibaraki 305-0044, Japan
[b] HREM Research Inc., 14-48 Matsukazedai, Higashimatsuyama, Saitama 355-0055, Japan

ARTICLE INFO

Article history:
Received 25 August 2016
Revised 13 March 2017
Accepted 17 March 2017
Available online xxx

Keywords:
STEM
Alignment
Ronchigram
Aberration

ABSTRACT

The aberrations of the objective lens should be measured and adjusted to realize high spatial resolution in scanning transmission electron microscopy (STEM). Here we report a method of measuring low-order aberrations using the Fourier transforms of Ronchigrams of an arbitrary crystal such as a specimen of interest. We have applied this technique to measure first- and second-order geometrical aberrations using typical standard specimens. Focus and twofold astigmatism are measured using two Ronchigrams obtained under different foci. Axial coma and threefold astigmatism are evaluated using the Fourier transforms of small subareas of a Ronchigram. The time dependences of focus and twofold astigmatism are examined using this technique for an aberration-corrected microscope.

1. Introduction

The alignment of an objective (probe-forming) lens system in scanning transmission electron microscopy (STEM) [1] is indispensable for performing high-resolution imaging and analysis, and the measurement of the objective-lens aberrations is critical for the alignment. For instance, a spherical aberration corrector [2] requires the measurement of the following aberrations; focus, twofold astigmatism, axial coma, threefold astigmatism, star, fourfold astigmatism and third-order spherical aberration. The lowest (first) order geometrical aberrations (i.e., focus and twofold astigmatism) should be frequently measured and realigned because of instrument and specimen instabilities, and the required precision of their measurement is on the order of nanometers. The second-order geometrical aberrations (i.e., axial coma and threefold astigmatism) are also important, although the required precision in measurements and their stabilities are relatively moderate compared with those for the first-order aberrations. The rapid measurement of lower-order aberrations using a specimen of interest is highly needed in actual applications because of the limited period of system stability.

Several aberration measurement methods have been developed that use annular dark-field (ADF) images or Ronchigrams. The method used for aberration correctors must measure high-order aberrations with high accuracy, and Ronchigram-based techniques (NION [3,4], JEOL [5]) and an ADF-image-based techniques (CEOS [6–8]) have been implemented in commercial products. Other relatively-rapid methods for measuring aberrations in STEM have also been developed [9–15] to meet the requirement for the instantaneous alignment of time-dependent low-order aberrations during experiments. The rapid regulation of time-dependent aberrations becomes critical for advanced applications, because the quantitative analyses of atomic ADF images require the values of aberrations at the time of imaging. For example, we reported quantitative analyses of graphene ADF images [16,17], and it was found that time-dependent low-order aberrations (e.g., axial coma) prevent advanced quantitative analyses.

This paper focuses on a rapid method of measuring low-order aberrations without using a specific specimen for alignment. This method is based on the Fourier transforms of Ronchigrams of an arbitrary crystalline specimen [18].

2. Outline of method

2.1. Theoretical background

There are several types of aberration notations in the field of STEM (e.g., [3,5,6,13]). Here we use the following notation of wave aberrations $\chi(u, v)$ in the orthogonal coordinates of angle (u, v) [13]:

$$\chi(u,v) = \frac{1}{2}C_1\left(u^2+v^2\right) + \frac{1}{2}\left\{A_{1a}\left(u^2-v^2\right) + 2A_{1b}uv\right\} + \left\{B_{2a}\left(u^3+uv^2\right) + B_{2b}\left(v^3+u^2v\right)\right\}$$

* Corresponding author.
E-mail address: kimoto.koji@nims.go.jp (K. Kimoto).

http://dx.doi.org/10.1016/j.ultramic.2017.03.021
0304-3991/

$$+\frac{1}{3}\left\{A_{2a}\left(u^3-3uv^2\right)+A_{2b}\left(3u^2v-v^3\right)\right\}$$
$$+\frac{1}{4}\left\{C_3\left(u^2+v^2\right)^2\right\}$$
$$+\frac{1}{4}\left\{A_{3a}\left(u^4-6u^2v^2+v^4\right)+4A_{3b}\left(u^3v-uv^3\right)\right\}$$
$$+\left\{S_{3a}\left(u^4-v^4\right)+2S_{3b}\left(u^3v+uv^3\right)\right\}$$
$$+\textit{higher order terms}, \tag{1}$$

where C_1, $\boldsymbol{A_1}$, $\boldsymbol{B_2}$, $\boldsymbol{A_2}$, C_3, $\boldsymbol{A_3}$ and $\boldsymbol{S_3}$ are, respectively, the focus, twofold astigmatism, axial coma, threefold astigmatism, third-order spherical aberration, fourfold astigmatism and star aberration, which is similar to the notation used in CEOS systems [6,7]. Overfocus is positive in this notation. Focus and third-order spherical aberration are scalar, but the other aberrations represented by bold characters are two-dimensional vectors, and thus have subscripts a and b. Note that the axial coma coefficient $\boldsymbol{B}_2$ is equal to one-third of the coefficients in the notation reported by Krivanek et al. [3], Sawada et al. [5] and Lupini [13].

It is known that the divergence of the wave aberration $\nabla\chi(u, v)$ is the geometrical aberration, which is the ray deviation on the specimen plane (x, y),

$$\begin{pmatrix}x\\y\end{pmatrix}=\nabla\chi(u,v). \tag{2}$$

Here we consider a Ronchigram in which the focus C_1 is larger than the ray deviation due to other aberrations in order to observe projected images (i.e., shadow imaging). Under such a focus condition (e.g. 300 nm), lattice distances projected on Ronchigram correspond to a small angle (e.g. less than 1 mrad). A small angular change (du, dv) on a Ronchigram causes a small displacement (dx, dy) of the ray on the specimen plane. Since the angular change (du, dv) is sufficiently small, we can use the Taylor expansion of Eq. (2) as follows [13]:

$$\begin{pmatrix}dx\\dy\end{pmatrix}\cong\boldsymbol{H}\begin{pmatrix}du\\dv\end{pmatrix},\quad \boldsymbol{H}=\begin{pmatrix}\frac{\partial^2\chi}{\partial u\partial u} & \frac{\partial^2\chi}{\partial u\partial v}\\ \frac{\partial^2\chi}{\partial v\partial u} & \frac{\partial^2\chi}{\partial v\partial v}\end{pmatrix}. \tag{3}$$

Here $\boldsymbol{H}$ is the Hessian matrix, which is a square matrix of the second-order partial derivatives of a scalar-valued function. Note that Eq. (3) is valid for a small angular change (du, dv); thus relatively large focus, which depends on residual aberrations, is indispensable. The Hessian matrix up to the second-order geometrical aberrations can be written as follows:

$$\boldsymbol{H}=\boldsymbol{H}_{C_1\boldsymbol{A}_1}+\boldsymbol{H}_{\boldsymbol{B}_2\boldsymbol{A}_2},$$

$$\boldsymbol{H}_{C_1\boldsymbol{A}_1}=\begin{pmatrix}C_1+A_{1a} & A_{1b}\\ A_{1b} & C_1-A_{1a}\end{pmatrix},$$

$$\boldsymbol{H}_{\boldsymbol{B}_2\boldsymbol{A}_2}=2\begin{pmatrix}(A_{2a}+3B_{2a})u+(A_{2b}+B_{2b})v & (A_{2b}+B_{2b})u-(A_{2a}-B_{2a})v\\ (A_{2b}+B_{2b})u-(A_{2a}-B_{2a})v & (-A_{2a}+B_{2a})u-(A_{2b}-3B_{2b})v\end{pmatrix}. \tag{4}$$

Eq. (3) can be rewritten as

$$\begin{pmatrix}du\\dv\end{pmatrix}=\boldsymbol{H}^{-1}\begin{pmatrix}dx\\dy\end{pmatrix}. \tag{5}$$

This equation indicates that a small displacement (dx, dy) on the specimen is projected on a small angular change (du, dv) on the Ronchigram multiplied by the inverse Hessian matrix $\boldsymbol{H}^{-1}$, which describes the local magnification of the Ronchigram. Most Ronchigram-based methods [3–5] utilize $\boldsymbol{H}^{-1}$ based on Eq. (5).

Here we consider the two-dimensional lattice of a crystalline specimen whose lattice vectors are $\boldsymbol{a}=\begin{pmatrix}a_x\\a_y\end{pmatrix}$ and $\boldsymbol{b}=\begin{pmatrix}b_x\\b_y\end{pmatrix}$ and whose distorted lattices observed on a Ronchigram are given by $\boldsymbol{p}=\begin{pmatrix}p_x\\p_y\end{pmatrix}$ and $\boldsymbol{q}=\begin{pmatrix}q_x\\q_y\end{pmatrix}$, respectively. Since the distorted lattice vectors ($\boldsymbol{p}$ and $\boldsymbol{q}$) on a defocused Ronchigram are very small, we can use Eq. (3) as follows:

$$\boldsymbol{a}=\boldsymbol{H}\boldsymbol{p}\quad\text{and}\quad\boldsymbol{b}=\boldsymbol{H}\boldsymbol{q}. \tag{6}$$

Using a sample lattice matrix $\boldsymbol{A}=\begin{pmatrix}a_x & b_x\\ a_y & b_y\end{pmatrix}=(\boldsymbol{a}\quad\boldsymbol{b})$ and a distorted lattice matrix $\boldsymbol{P}=\begin{pmatrix}p_x & q_x\\ p_y & q_y\end{pmatrix}=(\boldsymbol{p}\quad\boldsymbol{q})$, Eq. (6) can be combined to give

$$\boldsymbol{A}=\boldsymbol{H}\boldsymbol{P}. \tag{7}$$

An easy way to determine the distorted lattice parameters in a Ronchigram is to take a Fourier transform of the Ronchigram [11,13,14,18–20] and determine the two-dimensional reciprocal lattice. From the definition of the reciprocal lattice, the corresponding reciprocal-lattice matrix $\boldsymbol{P}^*$ satisfies

$$\boldsymbol{E}=\begin{pmatrix}\boldsymbol{p} & \boldsymbol{q}\end{pmatrix}^T\begin{pmatrix}\boldsymbol{p}^* & \boldsymbol{q}^*\end{pmatrix}=\boldsymbol{P}^T\boldsymbol{P}^*=(\boldsymbol{P}^*)^T\boldsymbol{P}$$

$$\boldsymbol{P}^{-1}=(\boldsymbol{P}^*)^T$$

where $\boldsymbol{E}$ is an identity matrix. Namely, the inverse of the lattice matrix $\boldsymbol{P}^{-1}$ is equal to the transposed reciprocal-lattice matrix $(\boldsymbol{P}^*)^{\mathrm{T}}$. Thus, Eq. (7) becomes

$$\boldsymbol{H}=\boldsymbol{A}(\boldsymbol{P}^*)^T. \tag{8}$$

Eq. (8) is the basic equation of our method. It should be emphasized that the Fourier transform of a Ronchigram is a direct way to measure the distorted reciprocal-lattice matrix $\boldsymbol{P}^*$ in Eq. (8).

To measure aberrations in $\boldsymbol{H}$ using Eq. (8), the sample lattice matrix $\boldsymbol{A}$ of the observed specimen should be known. The procedure used to measure aberrations without knowing the sample lattice matrix $\boldsymbol{A}$ is described in Appendix B. The sample lattice matrix $\boldsymbol{A}$ can be experimentally determined using two Ronchigrams whose difference in focus dC_1 is known. Note that the difference in $\boldsymbol{H}$ is simply $dC_1\boldsymbol{E}$ from Eq. (4) because other aberrations are the same. Furthermore, we evaluate the difference in $\boldsymbol{H}$ for the two Ronchigrams using Eq. (8) as follows:

$$\boldsymbol{H}_{C_1=C}-\boldsymbol{H}_{C_1=C+dC_1}=dC_1\boldsymbol{E}$$

$$=\boldsymbol{A}\left(\boldsymbol{P}^*_{C_1=C}\right)^{\mathrm{T}}-\boldsymbol{A}\left(\boldsymbol{P}^*_{C_1=C+dC_1}\right)^{\mathrm{T}}=\boldsymbol{A}(\Delta\boldsymbol{P}^*)^{\mathrm{T}},$$

where $\Delta\boldsymbol{P}^*$ is the difference between the two deformed reciprocal lattice matrices. It should be noted that this relation is valid even if higher-order aberrations exist. Thus, the sample lattice matrix $\boldsymbol{A}$ can be precisely obtained using the difference between two distorted lattice matrices $\Delta\boldsymbol{P}$ and the difference in focus dC_1 as follows:

$$\boldsymbol{A}=dC_1\left((\Delta\boldsymbol{P}^*)^{\mathrm{T}}\right)^{-1}=dC_1\Delta\boldsymbol{P}^{-1}. \tag{9}$$

Using the determined matrix $\boldsymbol{A}$, we can evaluate aberrations on the basis of Eq. (8). Since we need not to know the crystal lattice parameters in advance, the method can be used even with a specimen of interest. Ronchigram distortions caused by various post-specimen lenses are not problematic because they are similar to the static distortion of the specimen lattice. Even if the focus step of the instrument has a systematic deviation from the actual focus step, we can recalibrate the estimated aberration coefficients and reciprocal lattice vectors by multiplying by the factor of the deviation.

Please cite this article as: K. Kimoto, K. Ishizuka, Rapid measurement of low-order aberrations using Fourier transforms of crystalline Ronchigrams, Ultramicroscopy (2017), http://dx.doi.org/10.1016/j.ultramic.2017.03.021

Even after the determination of the sample lattice matrix $\boldsymbol{A}$, there may be various approaches to calculating aberration coefficients in $\boldsymbol{H}$, depending on the order of the aberrations to be evaluated. If the first-order geometrical aberrations are of interest, the segmentation of a Ronchigram is not very effective in terms of precision because it reduces the sampling resolution in the Fourier transforms. In the present study, we estimate the first-order geometrical aberrations from a whole Ronchigram and the second-order geometrical aberrations from several subareas.

2.2. Measurement of aberrations C_1, $\boldsymbol{A_1}$, $\boldsymbol{B_2}$ and $\boldsymbol{A_2}$

In the present study, we measure the following geometrical aberration coefficients up to the second order: focus C_1, twofold astigmatism $A_{1a,b}$, axial coma $B_{2a,b}$ and threefold astigmatism $A_{2a,b}$. First, we determine a sample lattice matrix $\boldsymbol{A}$ from Eq. (9). The prerequisite calibrated parameters are the focus step and camera length of Ronchigrams.

Using the sample lattice matrix $\boldsymbol{A}$, we determine the first-order aberration coefficients on the basis of Eq. (8) as follows:

$$\boldsymbol{H} \approx \boldsymbol{H}_{C_1\boldsymbol{A}_1} = \boldsymbol{A}(\boldsymbol{P}^*)^{\mathrm{T}}. \tag{10}$$

Here, we ignore geometrical aberrations higher than the first order. Full details of the equations used to calculate C_1 and $\boldsymbol{A_1}$ are given in Appendix A.

Next, we determine the second-order aberration coefficients. From Eq. (8), the difference between the Hessian matrices expected at two small subareas of a Ronchigram is given by

$$\boldsymbol{H}(\boldsymbol{k}_2) - \boldsymbol{H}(\boldsymbol{k}_1) = \boldsymbol{A}(\boldsymbol{P}_2^*)^{\mathrm{T}} - \boldsymbol{A}(\boldsymbol{P}_1^*)^{\mathrm{T}} = \boldsymbol{A}(\Delta\boldsymbol{P}^*)^{\mathrm{T}},$$

where $\boldsymbol{P}_1{}^*$ and $\boldsymbol{P}_2{}^*$ are the distorted reciprocal-lattice matrices of two small subareas in the Ronchigram whose centers are given by $\boldsymbol{k_1}$ and $\boldsymbol{k_2}$, respectively. Since the Hessian matrix for the first-order aberrations does not depend on the Ronchigram coordinates, the difference between the Hessian matrices for the second-order aberrations is given by the difference between the deformed reciprocal-lattice matrices $\Delta\boldsymbol{P}^*$ as shown below:

$$\begin{aligned}\boldsymbol{H}(\boldsymbol{k}_1) - \boldsymbol{H}(\boldsymbol{k}_2) &= \{\boldsymbol{H}_{C_1\boldsymbol{A}_1} + \boldsymbol{H}_{\boldsymbol{B}_2\boldsymbol{A}_2}(\boldsymbol{k}_1) + \cdots\} \\ &\quad -\{\boldsymbol{H}_{C_1\boldsymbol{A}_1} + \boldsymbol{H}_{\boldsymbol{B}_2\boldsymbol{A}_2}(\boldsymbol{k}_2) + \cdots\} \\ &\approx \boldsymbol{H}_{\boldsymbol{B}_2\boldsymbol{A}_2}(\boldsymbol{k}_1) - \boldsymbol{H}_{\boldsymbol{B}_2\boldsymbol{A}_2}(\boldsymbol{k}_2) = \boldsymbol{A}(\Delta\boldsymbol{P}^*)^{\mathrm{T}}\end{aligned} \tag{11}$$

Thus, the second-order geometrical aberrations can be evaluated using a single Ronchigram based on Eq. (11) using a sample matrix $\boldsymbol{A}$ when we ignore geometrical aberrations higher than the second order. The equations for calculating B_{2a}, B_{2b}, A_{2a} and A_{2b} are also given in Appendix A.

2.3. Example of procedure to measure aberrations

Here, we give an example of a procedure to measure the first-order aberration coefficients C_1 and $\boldsymbol{A_1}$ and the second-order aberration coefficients $\boldsymbol{B_2}$ and $\boldsymbol{A_2}$.

(a) A Ronchigram is acquired, and two spots $\boldsymbol{p}^*$ and $\boldsymbol{q}^*$ in the Fourier transform of the Ronchigram are selected. A distorted reciprocal-lattice matrix $\boldsymbol{P}_1{}^*$ is constructed. A nominal focus value is obtained from the microscope control software.
(b) The focus of the microscope is changed by dC_1. The two spots selected in (a) are tracked, and another distorted reciprocal-lattice matrix $\boldsymbol{P}_2{}^*$ is constructed.
(c) From the values of the focus change dC_1 and the difference $\Delta\boldsymbol{P}^*$ between the two distorted reciprocal-lattice matrices $\boldsymbol{P}_1{}^*$ and $\boldsymbol{P}_2{}^*$, the sample lattice matrix $\boldsymbol{A}$ is determined using Eq. (9).
(d) The first-order aberrations C_1 and $\boldsymbol{A_1}$ are calculated on the basis of Eq. (10). The equations used in the calculations are described in Appendix A. The difference between the actual focus and the nominal focus obtained in (a) defines the C_1 offset.
(e) (Optional) The measured $\boldsymbol{A_1}$ is corrected using a stigmator. The C_1 offset is corrected to adjust the nominal microscope focus to the actual focus.
(f) The second-order aberrations $\boldsymbol{B_2}$ and $\boldsymbol{A_2}$ are evaluated on the basis of Eq. (11), in which several subareas (e.g., $|\boldsymbol{k_1}|$, $|\boldsymbol{k_2}|\sim$20 mrad) of one Ronchigram are selected. The aberrations $\boldsymbol{B_2}$ and $\boldsymbol{A_2}$ can be evaluated from another Ronchigram, and we can take an average of them. The equations used in the calculations are described in Appendix A.
(g) (Optional) The measured $\boldsymbol{B_2}$ and $\boldsymbol{A_2}$ are corrected using an aberration corrector.
(h) (Optional) If necessary, return to step (a) for continuous aberration monitoring.

As mentioned above, the only experimental data required in this method are two Ronchigrams acquired at different foci. The typical processing time of steps (a)–(g) is less than 10 s, most of which comprises the exposure time and the intentional delay to stabilize the focus.

Note that these evaluated aberrations may differ from those measured by the aberration corrector because of the rotation and distortion of Ronchigrams due to post-specimen lenses. The evaluated aberrations using the present method can be converted to the aberrations in the aberration corrector system by measuring intentional aberration changes.

3. Experimental

We used an aberration-corrected microscope (FEI, Titan^3) at an acceleration voltage of 300 and 80 kV. Ronchigrams were acquired using a charge coupled device (CCD) camera attached in an energy filter (Gatan, GIF Quantum) without energy filtering. The procedures were performed using an in-house DigitalMicrograph (Gatan) script that can be applied with various Gatan cameras. A few typical TEM specimens were used: polycrystalline AuPd particles on an amorphous carbon film (Agar, Cross Grating Replica S106), a single crystal of $SrTiO_3$ prepared by Ar ion milling and a single-layer graphene.

4. Results and discussion

4.1. Experimental results

Fig. 1a and b show Ronchigrams of polycrystalline AuPd particles obtained at nominal foci of 213.7 nm (overfocus) and −213.7 nm (underfocus), respectively. The convergence semiangle is 42 mrad. The Fourier transforms of the Ronchigrams are shown in Fig. 1c and d, in which the brightness corresponds to each modulus. The positions of the distorted reciprocal lattices $\boldsymbol{p}^*$ and $\boldsymbol{q}^*$, shown as open circles, are evaluated with subpixel accuracy after convoluting a smoothing kernel (e.g., 7×7 pixels). The estimated twofold astigmatism $\boldsymbol{A_1}$ (A_{1a}, A_{1b}) is (1.1, 1.3) nm. The actual foci of the Ronchigrams (Fig. 1a and b) are found to be 217.2 nm and −210.2 nm, and thus the C_1 offset is 3.5 nm. It is worth mentioning that a single-crystal specimen is not necessary for the measurement of the first-order geometrical aberrations. Namely, the spots $\boldsymbol{p}^*$ and $\boldsymbol{q}^*$ and the corresponding lattice fringes may come from different domains of the Ronchigram. For example, we can use two spots $\boldsymbol{p}^*$ and $\boldsymbol{q}^*$ corresponding to differently oriented (100) fringes of independent domains. This is because the Hessian matrix for the first-order aberration does not depend on the position in a Ronchigram.

Please cite this article as: K. Kimoto, K. Ishizuka, Rapid measurement of low-order aberrations using Fourier transforms of crystalline Ronchigrams, Ultramicroscopy (2017), http://dx.doi.org/10.1016/j.ultramic.2017.03.021

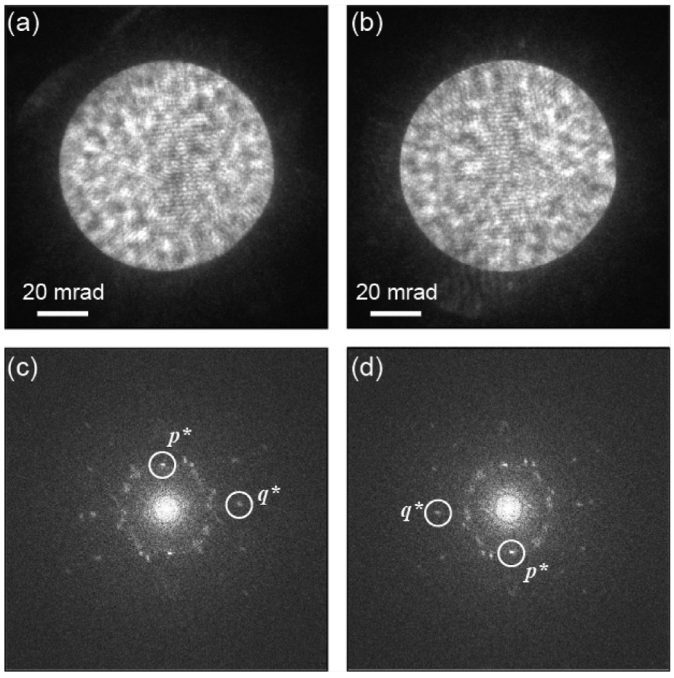

Fig. 1. Example of aberration measurement using polycrystalline AuPd grains. (a) and (b) Ronchigrams observed at nominal foci of 213.7 (overfocus) and −213.7 nm (underfocus), respectively. (c) and (d) Fourier transforms of Ronchigrams (a) and (b), respectively. Twofold astigmatism and focus offset are measured. The acceleration voltage was 300 kV.

The measurement of higher-order aberrations, however, requires a single crystal, which covers the areas where we determine the distorted lattices. This is because we use (or assume as in Appendix B) the same sample lattice matrix $\boldsymbol{A}$ for all the differently distorted lattices. Fig. 2a and b respectively show a Ronchigram and its Fourier transform obtained using a single-crystal $SrTiO_3$ specimen. The focus measured by the current method is 554.3 nm (overfocus). The open circles in Fig. 2a indicate the four subareas used to estimate the second-order geometric aberrations. The inset in Fig. 2b shows an enlarged −110 spot, whose intensity profile shown in Fig. 2c will be discussed in the Section 4.3. The estimated $\boldsymbol{A_1}$, $\boldsymbol{B_2}$ and $\boldsymbol{A_2}$ values in nanometers are (2.2, −0.3), $(0.5 \pm 2.7, 7.3 \pm 0.2)$ and $(-4.9 \pm 0.5, 5.4 \pm 0.1)$, respectively. Here, $\boldsymbol{B_2}$ and $\boldsymbol{A_2}$ are the averages of the values calculated from both Ronchigrams obtained at the overfocus shown here and an underfocus of −548.5 nm (not shown). Because the present experiments were performed with an aberration corrector, the third-order aberrations were corrected. Further studies for accuracy in $\boldsymbol{A_2}$ and $\boldsymbol{B_2}$ measurements are necessary particularly for the effects of higher-order aberrations.

One advantage of our method is its short processing time, and we can measure the stability of the low-order aberrations $\boldsymbol{A_1}$ and C_1 offset as shown in Fig. 3a. We have also plotted the measured sample lattice parameters in Fig. 3b. The measurement was performed using Ronchigrams of a single-crystal $SrTiO_3$ specimen as shown in the inset of Fig. 3a. The defocus in the Ronchigram observation was about ±577 nm, and the 110 and −110 spots were used for the measurement of $\boldsymbol{P}^*$. As shown in Fig. 3a and b, the experimental results showing high reproducibility suggest the high precision of our method.

Fig. 3a shows the changes in the twofold astigmatism $\boldsymbol{A_1}$, which were introduced using a spherical aberration corrector (i.e., so-called $\boldsymbol{A_1}$ coarse) during the stability measurement. An unexpected spike of the lattice angle was observed at about 5 min, which probably resulted from the change in the twofold astigmatism between the acquisitions of two Ronchigrams. Although we changed the twofold astigmatism by 10 nm using the aberration corrector, the measured astigmatisms are different from the target values. One of the reasons for this discrepancy is considered to be image distortion by the post-specimen lenses and the post-column energy filter. This is deduced from Fig. 3b, which indicates considerable distortion of the lattice parameters. Here, $|\boldsymbol{a}|$ and $|\boldsymbol{b}|$ are not equal and their angle is not 90°, although the −110 and 110 spots of $SrTiO_3$ were selected for $\boldsymbol{p}^*$ and $\boldsymbol{q}^*$.

Fig. 3a also indicates the high stability of first-order geometrical aberrations, which is on the order of 1 nm per minute. The aberration stability of TEM image correctors has been reported by Barthel and Thust [21], who pointed out the importance of low-order aberration stability. The stability shown in Fig. 3a is comparable to that of their advanced image corrector. In the case of TEM aberration measurement, the first-order geometrical aberrations can be estimated using a Fourier transform of one TEM image, while STEM aberration measurement requires at least two Ronchigrams (or a few ADF images), making STEM measurement time-consuming. It is worth mentioning that we can estimate aberrations using only a single Ronchigram if we know the sample lattice matrix $\boldsymbol{A}$ and other distortion factors due to post-specimen lenses.

This method can be used with ultrathin specimens such as a single-layer graphene. Fig. 4 shows the Ronchigrams of a single-

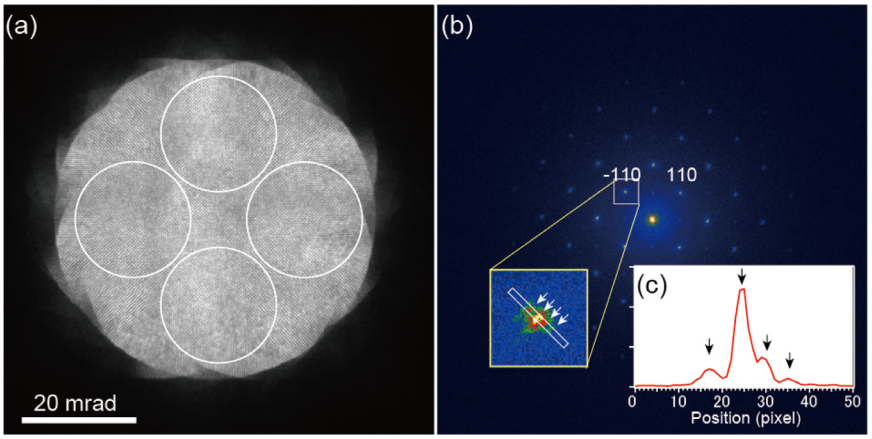

Fig. 2. (a) Ronchigram and (b) its Fourier transform for the assessment of aberrations C_1, $\boldsymbol{A_1}$, $\boldsymbol{B_2}$ and $\boldsymbol{A_2}$. The specimen was a $SrTiO_3$ (001) single crystal and the convergence semiangle was 28 mrad. The open circles in (a) show the subareas used for the measurements of $\boldsymbol{B_2}$ and $\boldsymbol{A_2}$. Inset of Fig. 2b shows the enlarged portion of the −110 spot. The intensity profile across the −110 spot is given in Fig. 2c. The acceleration voltage was 300 kV.

Please cite this article as: K. Kimoto, K. Ishizuka, Rapid measurement of low-order aberrations using Fourier transforms of crystalline Ronchigrams, Ultramicroscopy (2017), http://dx.doi.org/10.1016/j.ultramic.2017.03.021

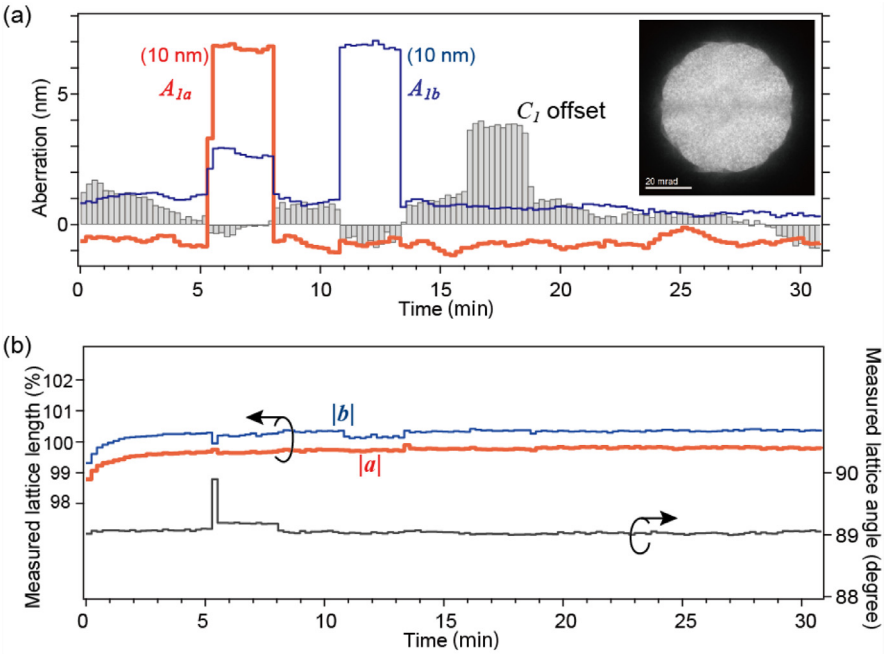

Fig. 3. Time dependences of measured C_1, $\boldsymbol{A_1}$ (a) and measured lattice vectors ***a, b*** (b). The inset of Fig. 3a shows a typical Ronchigram observed in these series of measurements. The specimen was a $SrTiO_3$ (001) single crystal and the acceleration voltage was 300 kV.

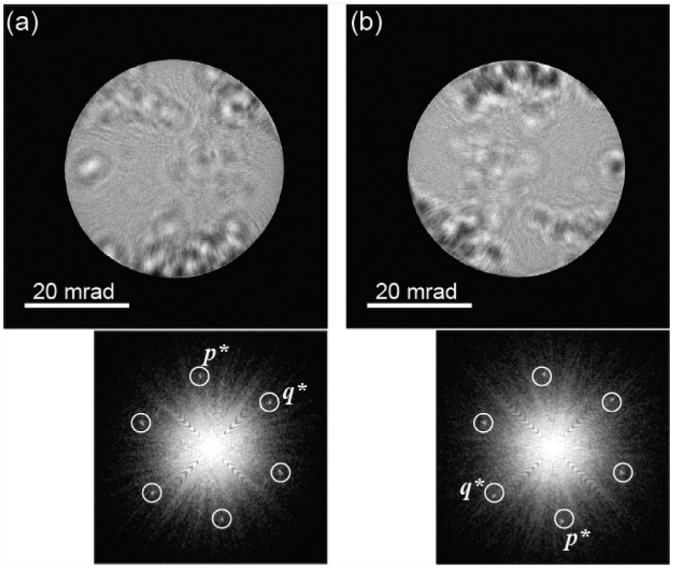

Fig. 4. Measurement of first-order aberrations using single-layer graphene specimen. Ronchigrams and their Fourier transforms observed under underfocus (a) and underfocus (b) conditions are shown. The acceleration voltage and the probe current were 80 kV and 27 pA, respectively. Fourier transforms of the Ronchigrams (lower figures) show hexagonal spots. Open circles are drawn at the same positions to clarify the difference in the spot positions between the two Fourier transforms (see off-centering of the spots in Fig. 4b).

layer graphene obtained at an acceleration voltage of 80 kV. An incident probe current and an exposure time were 27 pA and 1 s, respectively. The nominal foci of the two Ronchigrams are 301 and −301 nm. Although the Ronchigrams show intense contrast of surface contaminations, Fourier transforms (lower figures) show clear hexagonal spots. The C_1 offset and twofold astigmatism are found to be −1.0 nm and (3.3, −4.0) nm, respectively. Twofold astigmatism of a few nanometers has been detected as the difference of the hexagonal spot positions. Note that ADF image signal of a single-layer graphene is low (e.g., 0.05% using an ADF detector with an inner angle of 48 mrad [16,17]). The averaged ADF signal is estimated to be less than 4 electrons per pixel using a typical dwell time of 0.04 ms and an incident probe current of 27 pA. This means that the aberration measurement using such a low-intensity ADF image is not practical. Contrary, our method of low-order aberration measurement can be applicable even for various two-dimensional materials.

4.2. Comparison with other techniques and advantages of our method

We have proposed a rapid method for measuring low-order aberrations in STEM. The fundamental strategy of the present method [18] is similar to the segmented Ronchigram analysis reported by Lupini et al. [11], although the segmentation is optimized for the aberrations of interest. Since our method requires only two Ronchigrams, whose acquisition time is less than several seconds, it is relatively rapid in comparison with the technique based on ADF imaging. Our method theoretically relies on the Hessian matrix $\boldsymbol{H}$, while other methods based on the Ronchigram used by manufacturers (NION [3,4] and JEOL [5]) utilize the inverse Hessian matrix $\boldsymbol{H^{-1}}$. We may note that the optimum type of specimen is different for each method. For instance, a specimen that shows high contrast is preferable for the methods developed for CEOS and NION systems, and a homogeneous amorphous film is preferable for the method used in JEOL system. The present method uses a crystalline region, which often exists in a specimen of interest.

In general, the accuracy of aberration measurements depends on the response of the measured objects (e.g., the spots of Fourier transforms in our method) to the target aberrations. In the present method, the change in the first-order geometrical aberrations is linearly related to the position of the spots in the Fourier transform of a Ronchigram. The effects of the second-order geometrical aberrations are observed in the angular dependence of the deformed reciprocal-lattice matrices $\Delta\boldsymbol{P}^*$, in which the differences are proportional to the angle. These linear dependences make the evaluations reliable and simple.

Please cite this article as: K. Kimoto, K. Ishizuka, Rapid measurement of low-order aberrations using Fourier transforms of crystalline Ronchigrams, Ultramicroscopy (2017), http://dx.doi.org/10.1016/j.ultramic.2017.03.021

An atomic-resolved ADF image is highly affected by aberrations; however, the shape of the probe (e.g., full width at half maximum) does not linearly depend on aberrations C_1 and $\boldsymbol{A_1}$, mainly due to the effects of diffraction aberration near the in-focus condition. Furthermore, the ADF image of a crystalline specimen depends not only on the probe shape but also on other factors, such as electron channeling (dechanneling), cross talk between adjacent atomic columns, dynamical diffraction (e.g., [22]) and incident probe tilting [23]. Thus, it is not always easy to deduce the effects of aberrations from the atomic-resolved ADF image. In contrast to atomic-resolved ADF imaging, which requires small first-order aberrations (e.g., less than 10 nm order), Ronchigram observation can be performed with large first-order aberrations (e.g., 100 nm order). This is because the first-order geometrical aberrations do not reduce the visibility of interference fringes but they distort the fringes. Thus, Ronchigram observation is relatively robust, and our method can be used for rough alignment in which the large aberrations smear the contrast of high-resolution ADF images.

Finally, we note additional advantages of our method for practical use. 1) The Ronchigram-based method is useful for reducing beam damage or contamination, since a defocused probe used for Ronchigram acquisition is similar to the beam shower setting. 2) We can perform the alignment using faint interference fringes in Ronchigrams, even when the specimen suffers serious contamination. 3) Specimen misalignment from the zone axis and/or lateral specimen drift is not critical in Ronchigram observations, in contrast to ADF imaging. 4) The time dependence of the sample lattice matrix $\boldsymbol{A}$ (e.g., Fig. 3b) allows us to monitor changes in the specimen or fluctuations in the measurement technique.

4.3. Practical limitation of our method

We have recognized a few technical difficulties in the application of this method. One major difficulty lies in three-beam ($-\boldsymbol{g}$, $\boldsymbol{0}$ and $\boldsymbol{g}$) interference effect. This problematic interference effect yields intensity modulation at the spots as shown by arrows in Fig. 3b and c. This modulation has been explained as three-beam coherent convergent electron diffraction [20]. Due to the local-magnification dependence of the Ronchigram, the Fourier transform of a Ronchigram shows elongated spots whose intensity is modulated as shown in Fig. 3c. This intensity modulation is unavoidable even in the case of weak phase objects, although an acceptable measurement can be performed by the convolution of a kernel for smoothing, as demonstrated in the present study.

Other difficulty occurs owing to the dynamical diffraction effect in the case of thick specimens. The dynamical diffraction will result in a relative phase change in the diffracted waves as a function of the angle, and thus the position of the interference fringes will be shifted. If the angle that causes the relative phase change becomes comparable to the lattice fringe spacing in the Ronchigram, the observed fringe in the Ronchigram is no longer the expected distance based on the Bragg angle and the aberrations. Under such a strong diffraction condition, the Fourier transform of the Ronchigram shows broadened spots, and the precise determination of the spot positions becomes difficult. Intentional tilting of the crystal from the zone axis may be effective for reducing such a dynamical diffraction effect. Nevertheless, we have to avoid a thick sample for high-resolution studies.

5. Conclusion

We have reported an aberration measurement method based on the Fourier transforms of Ronchigrams. The method can be applied to any specimen that includes a crystalline domain. We demonstrated measurements of geometrical aberrations up to the second order, i.e., focus, twofold astigmatism, axial coma and threefold astigmatism. We also evaluated the time dependence of focus and twofold astigmatism, and high stability of about 1 nm/min was observed for twofold astigmatism on our microscope. As a final note, we are indebted to Ondrej Krivanek for the CCD camera [24] of the post-column energy filter [25,26] and the DigitalMicrograph script, which become indispensable tools for advanced electron microscopy.

Funding

This study was supported by the JST Research Acceleration Program and the Nanotechnology Platform of MEXT, Japan.

Acknowledgements

We thank Dr. Yamashita, Dr. Koshiya, Dr. Nagai, Dr. Kikkawa for invaluable discussions, and Dr. Suenaga for providing the graphene specimen. We also thank Dr. van Cappellen, Mr. Matsumoto, Dr. Jian and Dr. Freitag for the precise alignment of our Titan^3 microscope.

Appendix A. Examples of equations for calculating aberrations

The first-order geometrical aberrations C_1 and $\boldsymbol{A_1}$ are calculated using the following equations derived from Eqs. (4) and (10):

$$C_1 = \frac{1}{2}(a_x\ p_u + b_x\ q_u + a_y\ p_v + b_y\ q_v),$$

$$A_{1a} = \frac{1}{2}(a_x\ p_u + b_x\ q_u - a_y\ p_v - b_y\ q_v),$$

$$A_{1b} = a_y\ p_u + b_y\ q_u. \tag{A.1}$$

The second-order geometrical aberrations $\boldsymbol{B_2}$ and $\boldsymbol{A_2}$ are calculated from Eqs. (4) and (11) using the angular dependence of a distorted reciprocal-lattice matrix. Using the difference between the distorted reciprocal-lattice matrices $\Delta\boldsymbol{P_u}^*$ measured from two subareas separated by $2u_0$ along the $\boldsymbol{u}$ direction, we have the following equation:

$$\boldsymbol{A}\ (\Delta\boldsymbol{P_u}^*)^T = \begin{pmatrix} u_1 & u_3 \\ u_2 & u_4 \end{pmatrix},$$

where the right-hand side is the difference between the corresponding Hessian matrices. Then B_{2a} and A_{2a} are calculated using the following equations:

$$B_{2a} = \frac{1}{16\ u_0}(u_1 + u_4), \quad A_{2a} = \frac{1}{16u_0}(u_1 - 3u_4) \tag{A.2}$$

Similarly, from the difference between the distorted reciprocal-lattice matrices $\Delta\boldsymbol{P_v}^*$ measured from two subareas separated by $2v_0$ along the $\boldsymbol{v}$ direction, B_{2b} and A_{2b} are calculated using the following equations:

$$\boldsymbol{A}\ (\Delta\boldsymbol{P_v}^*)^T = \begin{pmatrix} v_1 & v_3 \\ v_2 & v_4 \end{pmatrix},$$

$$B_{2b} = \frac{1}{16\ v_0}(v_1 + v_4), \quad A_{2b} = \frac{1}{16\ v_0}(3v_1 - v_4). \tag{A.3}$$

Because the second-order geometrical aberrations $\boldsymbol{B_2}$ and $\boldsymbol{A_2}$ can be measured using each Ronchigram observed at overfocus or underfocus, we take the average of values measured from the two Ronchigrams.

Please cite this article as: K. Kimoto, K. Ishizuka, Rapid measurement of low-order aberrations using Fourier transforms of crystalline Ronchigrams, Ultramicroscopy (2017), http://dx.doi.org/10.1016/j.ultramic.2017.03.021

Appendix B. Procedure for measuring aberrations without calculating sample lattice matrix

Without determining a sample lattice matrix $\boldsymbol{A}$, we can derive a single equation from Eq. (6) for each distorted lattice parameter. Here, we obtain the distorted lattice parameters from the distorted reciprocal-lattice parameters. Therefore, we can use Eq. (7) to derive a simultaneous equation, where the aberration coefficients are the unknowns. In this Appendix, we describe calculation method without determining a sample lattice matrix.

The first-order aberration coefficients C_1 and $\boldsymbol{A_1}$ are determined using two Ronchigrams. From Eq. (7) we have the following equation between two distorted lattice matrices $\boldsymbol{P}_1$ and $\boldsymbol{P}_2$ determined from two Ronchigrams respectively observed at foci of C and $C+dC$:

$$\boldsymbol{A} \approx \boldsymbol{H}_{C_1\boldsymbol{A}_1}(C_1 = C)\boldsymbol{P}_1 \approx \boldsymbol{H}_{C_1\boldsymbol{A}_1}(C_1 = C + dC)\boldsymbol{P}_2, \tag{A.4}$$

where the second and higher-order aberrations are ignored. The second equality between the 2×2 matrices gives four simultaneous equations with three unknowns: C_1, A_{1a} and A_{1b}. Thus, we can determine these parameters from Eq. (A.4) in the sense of least square error. We have only a single equation, Eq. (A.4), for the pair of Ronchigrams taken at different foci since the Hessian matrix does not depend on the position of the Ronchigram. However, if we observe more than two Ronchigrams, we can derive a similar equation to Eq. (A.4) for each independent pair of Ronchigrams and solve them simultaneously with high accuracy using the least-squares technique.

The second-order aberration coefficients $\boldsymbol{B_2}$ and $\boldsymbol{A_2}$ are determined using several small subareas of a Ronchigram. From Eq. (7) we have the following equation for two distorted lattice matrices $\boldsymbol{P_i}$ and $\boldsymbol{P_j}$ obtained from two small areas i and j of a single Ronchigram:

$$\boldsymbol{A} = \boldsymbol{H}_{\boldsymbol{B}_2\boldsymbol{A}_2}(\boldsymbol{k_i})\boldsymbol{P_i} + \boldsymbol{H}_{C_1\boldsymbol{A}_1}\boldsymbol{P_i} \approx \boldsymbol{H}_{\boldsymbol{B}_2\boldsymbol{A}_2}(\boldsymbol{k_j})\boldsymbol{P_j} + \boldsymbol{H}_{C_1\boldsymbol{A}_1}\boldsymbol{P_j}, \tag{A.5}$$

where the third and higher-order geometrical aberrations are ignored. Here, $\boldsymbol{k}_i$ and $\boldsymbol{k}_j$ denote the center positions of the two small subareas in the Ronchigram. If we use the first-order aberration coefficients determined above, the two distorted lattice matrices from the two small subareas give four simultaneous equations with four unknowns (B_{2a}, B_{2b}, A_{2a} and A_{2b}). Thus, we can determine these parameters uniquely from Eq. (A.5).

If we measure the distorted lattice matrices from more than two different subareas of the Ronchigram, we can derive similar equations to Eq. (A.5) for independent pairs of the distorted lattice matrices. For example, if we measure three distorted lattice matrices from three small subareas, we have the following two equations:

$$\begin{aligned}\boldsymbol{H}_{\boldsymbol{B}_2\boldsymbol{A}_2}(\boldsymbol{k}_1)\boldsymbol{P}_1 + \boldsymbol{H}_{C_1\boldsymbol{A}_1}\boldsymbol{P}_1 &= \boldsymbol{H}_{\boldsymbol{B}_2\boldsymbol{A}_2}(\boldsymbol{k}_2)\boldsymbol{P}_2 + \boldsymbol{H}_{C_1\boldsymbol{A}_1}\boldsymbol{P}_2,\\ \boldsymbol{H}_{\boldsymbol{B}_2\boldsymbol{A}_2}(\boldsymbol{k}_1)\boldsymbol{P}_1 + \boldsymbol{H}_{C_1\boldsymbol{A}_1}\boldsymbol{P}_1 &= \boldsymbol{H}_{\boldsymbol{B}_2\boldsymbol{A}_2}(\boldsymbol{k}_3)\boldsymbol{P}_3 + \boldsymbol{H}_{C_1\boldsymbol{A}_1}\boldsymbol{P}_3,\end{aligned} \tag{A.6}$$

which give eight simultaneous equations with seven or four unknowns if we include or exclude the first-order aberrations, respectively. Thus, we can determine all these parameters from Eq. (A.6) in the sense of least square error. We can easily perform extra measurements of the distorted lattice matrices from different subareas of a single Ronchigram, and derive similar equations to Eq. (A.6) for independent pairs of different subareas. Note that we can derive Eq. (A.6) for each Ronchigram. By solving these equations simultaneously using the least-squares technique, we can determine the first- and second-order aberration coefficients simultaneously with high accuracy.

References

[1] S.J. Pennycook, P.D. Nellist, Scanning transmission electron microscopy, Imaging and Analysis, Springer, New York, 2011.
[2] P.W. Hawkes, Aberration-Corrected Electron Microscopy, Elsevier, New York, 2008.
[3] O.L. Krivanek, N. Dellby, A.R. Lupini, Ultramicroscopy 78 (1999) 1–11.
[4] N. Dellby, O.L. Krivanek, P.D. Nellist, P.E. Batson, A.R. Lupini, J. Electron Microsc. 50 (2001) 177–185.
[5] H. Sawada, T. Sannomiya, F. Hosokawa, T. Nakamichi, T. Kaneyama, T. Tomita, Y. Kondo, T. Tanaka, Y. Oshima, Y. Tanishiro, K. Takayanagi, Ultramicroscopy 108 (2008) 1467–1475.
[6] M. Haider, H. Müller, S. Uhlemann, Present and future hexapole aberration correctors for high-resolution electron microscopy, in: Peter W. Hawkes (Ed.), Advances in Imaging and Electron Physics, Elsevier, New York, 2008, pp. 43–119.
[7] P. Hartel, H. Müller, S. Uhlemann, M. Haider, in: Microscopy and Microanalysis, 13, Cambridge University Press, 2007, pp. 1148–1149.
[8] S. Uno, K. Honda, N. Nakamura, M. Matsuya, J. Zach, Optik 116 (2005) 438–448.
[9] Q.M. Ramasse, A.L. Bleloch, Ultramicroscopy 106 (2005) 37–56.
[10] H. Sawada, M. Watanabe, I. Chiyo, Microsc. Microanal. 18 (2012) 705–710.
[11] A.R. Lupini, S.J. Pennycook, J. Electron Microsc. 57 (2008) 195–201.
[12] A.R. Lupini, P. Wang, P.D. Nellist, A.I. Kirkland, S.J. Pennycook, Ultramicroscopy 110 (2010) 891–898.
[13] A.R. Lupini, TheElectron Ronchigram, in: Stephen J. Pennycook, Peter D. Nellist (Eds.), Scanning Transmission Electron Microscopy, Springer, New York, 2011, pp. 117–161.
[14] K. Kuramochi, T. Yamazaki, Y. Kotaka, Y. Kikuchi, I. Hashimoto, K. Watanabe, Ultramicroscopy 108 (2008) 339–345.
[15] H. Akima, T. Yoshida, Microscopy 63 (2014) 325–332.
[16] S. Yamashita, S. Koshiya, K. Ishizuka, K. Kimoto, Microscopy 64 (2015) 143–150.
[17] S. Yamashita, S. Koshiya, T. Nagai, J. Kikkawa, K. Ishizuka, K. Kimoto, Microscopy 64 (2015) 409–418.
[18] K. Kimoto, K. Ishizuka, Y. Matsui, Patent, PCT/JP2007/000455 WO 2007/125652 A1 (2007)
[19] C.B. Boothroyd, Scan. Microsc. 11 (1997) 31–42.
[20] K. Ishizuka, K. Kimoto, Y. Bando, Microsc. Microanal. 15 (2009) 1094–1095.
[21] J. Barthel, A. Thust, Ultramicroscopy 134 (2013) 6–17.
[22] K. Kimoto, T. Asaka, X. Yu, T. Nagai, Y. Matsui, K. Ishizuka, Ultramicroscopy 110 (2010) 778–782.
[23] Y.G. So, K. Kimoto, J. Electron Microsc. 61 (2012) 207–215.
[24] O.L. Krivanek, P.E. Mooney, Ultramicroscopy 49 (1993) 95–108.
[25] O.L. Krivanek, M.K. Kundmann, K. Kimoto, J. Microsc. 180 (1995) 277–287.
[26] O.L. Krivanek, A.J. Gubbens, N. Dellby, Microsc. Microanal. Microstruct. 2 (1991) 315–332.

Please cite this article as: K. Kimoto, K. Ishizuka, Rapid measurement of low-order aberrations using Fourier transforms of crystalline Ronchigrams, Ultramicroscopy (2017), http://dx.doi.org/10.1016/j.ultramic.2017.03.021